

Electronic Supplementary Material

Inherited IRAK-4 deficiency in acute human herpesvirus-6 encephalitis

Zeynep Güneş Tepe^{1,†}, Yılmaz Yücehan Yazıcı^{1,†}, Umut Tank¹, Ladin Işık Köse¹,
Murat Özer², Caner Aytekin², and Serkan Belkaya^{1,*}

¹Department of Molecular Biology and Genetics, Faculty of Science, İhsan Doğramacı Bilkent University, Ankara, Turkey.

²Department of Pediatric Immunology, Dr. Sami Ulus Maternity and Children's Health and Diseases Training and Research Hospital, Ankara, Turkey.

† Equal contribution

*Correspondence
Serkan Belkaya, PhD
E-mail: sbelkaya@bilkent.edu.tr

This electronic supplementary file includes:

Supplementary Material and Methods

Supplementary Tables 1, 2, 3, 4, 5, 6

Supplementary Figures 1, 2

Supplementary References

Supplementary Materials and Methods

RNA extraction and gene expression analysis

For cloning purposes, cDNA samples were generated with iScript cDNA Synthesis kit (BioRad, USA) using total RNA isolated from various cells using GeneJET RNA Purification kit (Thermo Fisher Scientific, USA). For real-time quantitative PCR (RT-qPCR), total RNA isolated from PBMCs was used to generate cDNA with the RevertAid First-Strand cDNA Synthesis System (Thermo Fisher Scientific) using oligo-dT primer. cDNA samples were amplified using the LightCycler 480 SYBR Green I Master kit (Roche, USA) on an LightCycler 96 Real-Time PCR system (Roche). Relative gene expression was calculated by the 2^{-ddC_t} method. Primers are provided in Table S1.

Molecular dynamics (MD) simulation and analysis of MD trajectories

The structure and atomic coordinate of the human IRAK-4 death domain (DD) were obtained from the Protein Data Bank (PDB ID: 3MOP) (Lin et al., 2010). The crystal structure contains 4 IRAK-4 DDs within Myd88 and IRAK-2 assembly and all IRAK-4 chains were similar, with no missing amino acid or unmodeled regions reported. The p.C79Y mutation was introduced to the WT IRAK-4 DD structure and refined via FoldX repair command (Schymkowitz et al., 2005). The structures were put into a dodecahedron box with water molecules and periodic boundary conditions were set. All systems were neutralized by Na^+ and Cl^- ions and minimized with 50,000 steps of steepest descent. Initially, for the NVT ensemble, a modified Berendsen thermostat with no pressure coupling was applied for both systems for 100 ps at 300 K. and Particle Mesh Ewald (PME) method was used to calculate electrostatic interactions (Berendsen et al., 1984; Essmann et al., 1995). Resulting systems with either WT or mutant IRAK-4 DD were simulated by GROMACS (Groningen Machine for Chemical Simulations) (<http://www.gromacs.org/>) using the CHARMM36 force field with an integration time-step of 2 fs (Huang et al., 2017). Water was treated explicitly using the TIP3P model (Jorgensen et al., 1983). After 100 ps of NPT equilibration at 300 K, production simulations were lasted for 100 ns at the same temperature. Analyses of trajectories were done using Visual Molecular Dynamics (VMD) to calculate the root mean square deviation (RMSD), root means square fluctuation (RMSF), and radius of gyration (R_g) of backbone atoms (Humphrey et al., 1996). The hydrogen bond number, solvent accessible surface (SASA), and Free energy landscape (FEL) for the first two eigenvectors were calculated using utilities provided in GROMACS v2021.1. The analyses of secondary structure were done by using the MDTraj “compute_dssp” module (McGibbon et al., 2015). Visuals were produced by using representative structures obtained from the last 1 ns of simulations using VMD. The PRODIGY (Protein binding energy prediction) server was used to determine the residues found in the Myd88 and IRAK-4 interaction site in the 3MOP (Xue et al., 2016). The docking was performed for the WT and mutant (p.C79Y) IRAK-4 DD obtained from MD simulation with Myd88 obtained from the crystal structure (PDB ID: 3MOP) (Lin et al., 2010), using the default setting in the HADDOCK 2.4 server (van Zundert et al., 2016).

Table S1. List of primers used in this study

IRAK4 gDNA Fwd	CAGAACCGTGAGCCAAATTAAC	Sanger sequencing (C79Y)
IRAK4 gDNA Rev	CCTAATTGTGGACACCCCTGG	Sanger sequencing (C79Y)
IRAK4_WT_Fwd BamHI	GACGGATCCATGGATTACAAGGATGACGACGATAA GATGAACAAACCCATAACACC	Cloning (pcDNA3.1)
IRAK4_WT_Rev XhoI	GCATCTCGAGTTAAGAACGCTGTCATCTCTTG	Cloning (pcDNA3.1)
IRAK4_Seq1_Fwd	CCACCTGACTCCTCAAGTCC	Sanger sequencing (IRAK4 ORF)
IRAK4_Seq2_Rev	GGACTTGAGGAGTCAGGTGG	Sanger sequencing (IRAK4 ORF)
IRAK4_Seq3_Fwd	GAATAGCAGAATTGTGGGAAC	Sanger sequencing (IRAK4 ORF)
IRAK4_Seq4_Rev	GTTCCCACAATTCTGCTAGTC	Sanger sequencing (IRAK4 ORF)
IRAK4_C79Y_SDm_Fwd	GCACCACAAATTACACAGTTGGTG	SDM (pcDNA3.1)
IRAK4_C79Y_SDm_Rev	CACCAACTGTGTAATTGTGGTGC	SDM (pcDNA3.1)
IRAK4_R12C_SDm_Fwd	CCATCACACATATGTGTGCTGCCCT	SDM (pcDNA3.1)
IRAK4_R12C_SDm_Rev	GAGGCAGCACACATATGTTGATGG	SDM (pcDNA3.1)
IRAK4 SDM Fwd	CGGGACTTCCAAAATGTCGT	SDM (pcDNA3.1)
IRAK4 SDM Rev	GGCACCTCCAGGGTCAAGG	SDM (pcDNA3.1)
IRAK4_EcoRI_Fwd N3XF	GCTGGAATTGATGAACAAACCCATAACACC	Subcloning (pCI-neo-N-3xFLAG)
IRAK4_XbaI_Rev N3XF	CTTCTAGATTAAGAACGCTGTCATCTCTTG	Subcloning (pCI-neo-N-3xFLAG)
IL18RAP HindIII Fwd	ACGAAGCTTCATGCTCTGTTGGCTG	Cloning (pCMV6)
IL18RAP_XhoI_Rev	AGGGCTCGAGTCACCATTCTTAGGCTGG	Cloning (pCMV6)
IL18RAP_Seq1_Fwd	CCTACTTCTGGGAGCACTG	Sanger Sequencing (IL18RAP)
IL18RAP_Seq2_Rev	CAGTGCTCCCAAGAACGAGTAGG	Sanger Sequencing (IL18RAP)
IL18RAP_Seq3_Fwd	GAAATAGTGCTGCTGTACCG	Sanger Sequencing (IL18RAP)
IL18RAP_Seq4_Rev	CGGTACAGCAGCACTATTTC	Sanger Sequencing (IL18RAP)
IRAK4_gRNA1_Fwd ^a	CACCGTATGTGCGCTGCCTCAATG	Cloning (CRISPR)
IRAK4_gRNA1_Rev ^a	AAACACATTGAGGCAGCGCACATAC	Cloning (CRISPR)
IRAK4_gRNA2_Fwd ^a	CACCGAGGCAGCGCACATATGTTGA	Cloning (CRISPR)
IRAK4_gRNA2_Rev ^a	AAACTCAACATATGTGCGCTGCCCT	Cloning (CRISPR)
IRAK4 CRISPR_Out Fwd	GTGGAAAAAGGAAGCAAACC	Competitive PCR (CRISPR)
IRAK4 CRISPR_Out Rev	AGCAACAACTTAAACGTCA	Competitive PCR (CRISPR)
IRAK4 CRISPR1_In Fwd (F1)	GTGCGCTGCCTCAATGT	Competitive PCR (CRISPR)
IRAK4 CRISPR1_In Rev (R1)	CAGCTTCTTAATTAGTCCAACA	Competitive PCR (CRISPR)
IRAK4 CRISPR2_In Fwd (F2)	GAACAAACCCATAACACCATCA	Competitive PCR (CRISPR)
IRAK4 CRISPR2_In Rev (R2)	GCAGCGCACATATGTTGA	Competitive PCR (CRISPR)
IRAK4_cDNA_Fwd ^b	TGGCAAAGTGTCAACATGAAAAC	Gene expression (RT-qPCR)
IRAK4_cDNA_Rev ^b	GGTGGAGTACCATCCAAGCAA	Gene expression (RT-qPCR)
HPRT1_cDNA_Fwd ^c	CTGGCGCTGTGATTAGTGATGATG	Gene expression (RT-qPCR)
HPRT1_cDNA_Rev ^c	TTGAGCACACAGAGGGCTACAATG	Gene expression (RT-qPCR)

Fwd: Forward, Rev: Reverse

^a(Jordi et al., 2017)^bPrimerBank ID: 223671887c2^c(Belkaya et al., 2019)

Table S2. List of antibodies used in this study

Antibody	Clone or Catalog #	Company	Purpose
anti-FLAG	M2	Sigma-Aldrich, USA	Immunoblotting
anti-human GAPDH	1E6D9	Proteintech, USA	Immunoblotting
anti-GFP	JL-8	Clontech, Japan	Immunoblotting
Goat anti-Mouse IgG	72-8062-M001	Tonbo Biosciences, USA	Immunoblotting
anti-human IRAK4 Alexa Fluor 647	L29-525	BD Biosciences, USA	Immunoblotting Flow cytometry
anti-human CD3 Pacific Blue	OKT3	Biolegend, USA	Flow cytometry
anti-human CD4 FITC	OKT4	Biolegend, USA	Flow cytometry
anti-human CD8 PE	HIT8a	Biolegend, USA	Flow cytometry
anti-human CD14 FITC	M5E2	Biolegend, USA	Flow cytometry
anti-human CD19 PE	HIB19	Biolegend, USA	Flow cytometry
anti-human TNF APC	MAb11	Biolegend, USA	Flow cytometry
anti-mouse IgG1 APC	MOPC-21	Biolegend, USA	Flow cytometry
anti-mouse IgG1 Alexa Fluor 647	MOPC-21	BD Biosciences, USA	Flow cytometry

Antibody dilutions were used according to the manufacturer's recommendations.

Table S3. Genetic analysis of the WES data of the patient

Number of annotated variants (Number of mutated genes)	Patient
Total	147225 (22483)
Nonsynonymous and essential splicing	11943 (6029)
MAF <1%	496 (448)
Homozygous	24 (24)

The table shows the number of annotated variations with the number of genes, shown in parenthesis, found in the patient. The low-quality variants with low depth coverage (variants with Reads <5, Mapping Quality <40, and Genotype Quality <30) were excluded. All variants except nonsynonymous (missense, insertion, deletion, start-loss, stop-loss, stop-gain) and essential splicing (± 2 bp from the exon-intron boundary) were excluded. Variants with a higher MAF of 1% in population databases (gnomAD and 1000G), including subpopulations (African, Ashkenazi Jewish, Finnish, non-Finnish European, South Asian, East Asian, and Latino) in gnomAD were excluded.

Table S4. Homozygous rare nonsynonymous variants found in the patient

GENE	GDI ^a	Variation		Zygosity	MAF	In silico Damage Prediction			gnomAD # Hom ^b	gnomAD pLoF # Hom ^c
		Type	Change			CADD/MSC	SIFT	PolyPhen-2		
CPA3	4.26	Missense	ENST00000296046:p.Arg237His	HOM	1.56E-04	26.5/11.2	D	D	0	0
HPS3	3.26	Missense	ENST00000296051:p.Arg822Gln	HOM	7.98E-06	22.5/22.3	B	D	0	0
IGSF10	5.96	Stop Gain	ENST00000282466:p.Gln1828*	HOM	1.19E-05	38/25	NA	NA	0	0
PCDHGA6	3.90	Frameshift	ENST00000517434:p.Gln772fs	HOM	3.98E-06	24.7/12.7	NA	NA	0	1
SPRY4	2.31	Missense	ENST00000344120:p.Lys177Arg	HOM	1.61E-03	22.2/16.1	B	B	0	0
OR5M8	2.57	Missense	ENST00000327216:p.Ala105Thr	HOM	3.89E-05	0.003/20.2	B	B	0	0
MRPS35	4.95	Missense	ENST00000081029:p.Tyr27Cys	HOM	1.74E-04	7.69/16.5	B	B	1	1
IRAK4	5.20	Missense	ENST00000448290:p.Cys79Tyr	HOM	-	28/15.2	D	D	0	0
KMT2D	6.74	Missense	ENST00000301067:p.Gln3269Arg	HOM	-	23.4/17.3	B	D	0	0
SMARCD1	0.68	Missense	ENST00000394963:p.Val278Met	HOM	4.52E-04	23/22.2	B	B	1	0
ACAN	26.89	Missense	ENST00000439576:p.Gly1374Arg	HOM	6.07E-03	13.03/18	B	B	1	0
KRTAP2-2	6.42	Frameshift	ENST00000542910:p.Pro91fs	HOM	1.92E-05	33/ND	NA	NA	0	0
TMPRSS9	16.19	Missense	ENST00000332578:p.Arg852Cys	HOM	2.01E-04	26.1/11.2	B	D	0	2
SAFB	1.28	Missense	ENST00000588852:p.Ile126Val	HOM	7.95E-06	15.18/10	B	B	0	0
FUT3	10.86	Missense	ENST00000303225:p.Asp96Asn	HOM	1.99E-05	6.979/13.7	B	B	0	0
LTBP4	21.48	Missense	ENST00000308370:p.Gly650Asp	HOM	-	29.7/23	D	D	0	0
CCDC97	1.15	Missense	ENST00000269967:p.Ala65Thr	HOM	3.98E-06	22.6/12.1	B	D	0	0
DEDD2	0.92	Missense	ENST00000595337:p.Gly318Val	HOM	5.69E-04	17.93/12.7	D	B	0	0
ZNF404	14.45	Missense	ENST00000587539:p.His209Tyr	HOM	8.18E-05	24.4/15.7	D	D	0	0
ZNF226	4.21	Missense	ENST00000337433:p.Thr666Ala	HOM	7.98E-06	22.9/11.4	D	B	0	0
PRR12	3.89	Missense	ENST00000418929:p.Ala1427Val	HOM	1.80E-04	12.85/22.8	B	B	1	0
TSKS	9.20	Missense	ENST00000246801:p.Arg371Trp	HOM	1.34E-03	25.1/24.8	B	D	2	0
MYH14	7.88	Missense	ENST00000262269:p.Arg1531Gln	HOM	4.07E-06	24.6/20.1	B	D	0	0
KLK11	5.27	Missense	ENST00000594768:p.Arg140His	HOM	1.34E-04	23.3/11.3	B	B	0	0

^aGene damage index (GDI) describes the least mutated and most mutated genes in the range of 0.0001 to 42.91.

^bThe number of homozygote individuals in gnomAD carrying the same variant found in the patient.

^cNumber of potential loss of function (pLoF) variants (insertion, deletion, start-loss, stop-loss, stop-gain, essential-splicing), for which there are homozygote carriers found in the gnomAD for the genes indicated.

D: Damaging. B: Benign. HOM: Homozygous. NA: Not Applicable.

Table S5. Characteristics of genes with homozygous rare nonsynonymous variations present in the patient

Gene description	Expression pattern	Known function	Clinical significance
Carboxypeptidase A3 (<i>CPA3</i>)	Biased expression in gallbladder and lung.	Degradation of endogenous proteins and the inactivation of venom-associated peptides.	Unknown
HPS3 Biogenesis Of Lysosomal Organelles Complex 2 Subunit 1 (<i>HPS3</i>)	Broad expression in liver, lymph node and other tissues.	Involved in the biogenesis of melanosomes, platelet dense granules, and lysosomes.	Biallelic mutations cause Hermansky-Pudlak syndrome 3.
Immunoglobulin Superfamily Member 10 (<i>IGSF10</i>)	Broad expression in gall bladder, ovary and other tissues.	Regulates the migration of neurons expressing gonadotropin releasing hormone.	Unknown
Protocadherin Gamma Subfamily A, 6 (<i>PCDHGA6</i>)	Biased expression in brain.	Involved in the establishment of specific neuronal connections in the brain.	Unknown
Sprouty RTK Signaling Antagonist 4 (<i>SPRY4</i>)	Broad expression in lung, adrenal and other tissues.	Encodes an inhibitor of the receptor-transduced mitogen-activated protein kinase (MAPK) signaling pathway.	Mutations cause hypogonadotropic hypogonadism 17 with or without anosmia.
Olfactory Receptor Family 5 Subfamily M Member 8 (<i>OR5M8</i>)	Expression in Olfactory Mucosa.	Encoded protein is responsible for the recognition and G protein-mediated transduction of odorant signals.	Unknown
Mitochondrial Ribosomal Protein S35 (<i>MRPS35</i>)	Ubiquitous expression in kidney, colon and other tissues.	Involved in protein synthesis within the mitochondrion.	Unknown
Interleukin 1 Receptor Associated Kinase 4 (<i>IRAK4</i>)	Ubiquitous expression in lymph node, appendix and other tissues.	Encodes a kinase that activates NF-kappaB in both the Toll-like receptor and T-cell receptor signaling pathways.	Biallelic mutations cause recurrent severe systemic and invasive bacterial infections.
Lysine Methyltransferase 2D (<i>KMT2D</i>)	Ubiquitous expression in bone marrow, skin and other tissues.	Encodes a histone methyltransferase that regulates the beta-globin and estrogen.	Mutations cause Kabuki syndrome 1.
SWI/SNF related, matrix associated, actin dependent regulator of chromatin, subfamily d, member 1 (<i>SMARD1</i>)	Ubiquitous expression in lymph node, testis and other tissues.	Thought to regulate transcription of certain genes by altering the chromatin structure around those genes.	Mutations cause Coffin-Siris syndrome 11.
Aggrecan (<i>ACAN</i>)	Broad expression in testis, urinary bladder and other tissues.	Encoded protein is an integral part of the extracellular matrix in cartilaginous tissue and it withstands compression in cartilage.	Biallelic mutations cause spondyloepimetaphyseal dysplasia, aggrecan type.
Keratin Associated Protein 2-2 (<i>KRTAP2-2</i>)	Distinct expression in the hair cortex.	May involve in keratinization	Unknown
Transmembrane Serine Protease 9 (<i>TMPRSS9</i>)	Broad expression in spleen, testis and other tissues.	Encodes a membrane-bound type II serine protease.	Unknown
Scaffold Attachment Factor B (<i>SAFB</i>)	Ubiquitous expression in spleen, testis and other tissues.	Encodes a DNA-binding protein which has high specificity for scaffold or matrix attachment region DNA elements (S/MAR DNA).	Unknown
Fucosyltransferase 3 (<i>FUT3</i>)	Biased expression in colon, esophagus and other tissues.	Catalyzes the addition of fucose to precursor polysaccharides.	Mutations cause Lewis antigen-negative phenotypes.
Latent Transforming Growth Factor Beta Binding Protein 4 (<i>LTBP4</i>)	Broad expression in prostate, endometrium and other tissues.	Encoded protein binds transforming growth factor beta as it is secreted and targeted to the extracellular matrix.	Biallelic mutations cause cutis laxa, autosomal recessive, type IC.
Coiled-Coil Domain Containing 97 (<i>CCDC97</i>)	Ubiquitous expression in testis, ovary and other tissues.	Unknown	Unknown
Death Effector Domain Containing 2 (<i>DEDD2</i>)	Enhanced expression in bone marrow, broad expression in spleen and other tissues.	Functions in the extrinsic apoptosis pathway and regulate nuclear breakdown	Unknown
Zinc Finger Protein 404 (<i>ZNF404</i>)	Ubiquitous expression in brain, testis, and other tissues.	Predicted to be involved in transcriptional regulation.	Unknown
Zinc Finger Protein 226 (<i>ZNF226</i>)	Ubiquitous expression in prostate, thyroid, and other tissues.	Predicted to be involved in transcriptional regulation.	Unknown
Proline Rich 12 (<i>PRR12</i>)	Ubiquitous expression in spleen, fat and other tissues.	Thought to be involved in nervous system development.	Mutations cause neuro-ocular syndrome.
Testis Specific Serine Kinase Substrate (<i>TSKS</i>)	Restricted expression toward testis.	Involved in testicular physiology, spermatogenesis or spermiogenesis.	Unknown
Myosin Heavy Chain 14 (<i>MYH14</i>)	Broad expression in colon, duodenum and other tissues.	Encodes a conventional non-muscle myosin.	Mutations cause deafness, autosomal dominant 4A.
Kallikrein Related Peptidase 11 (<i>KLK11</i>)	Biased expression in esophagus, skin, and other tissues.	Encodes one of the fifteen kallikrein subfamily members as a subgroup of serine proteases	Unknown

Expression pattern, function, and clinical significance of genes were obtained by using the NCBI (<https://www.ncbi.nlm.nih.gov/>), Protein Atlas (<https://www.proteinatlas.org/>) and OMIM (<https://www.omim.org/>) databases.

Table S6. Disease-causing variations in *IRAK4*

Variation	Zygosity	CADD	References
NM_016123.4:c.1A>G:NP_057207.2:p.M1V	COMP HET	23.6	Ku et al., 2007
NM_016123.4:c.29_30delAT:NP_057207.2:p.Y10Cfs*9	COMP HET	29.1	Nishimura et al., 2021
NM_016123.4:c.34C>T:NP_057207.2:p.R12C	COMP HET	28.9	Hoarau et al., 2007
NM_016123.4:c.35G>C:NP_057207.2:p.R12P	COMP HET	28.5	Nishimura et al., 2021
NM_016123.4:c.123dup:NP_057207.2:p.P42Tfs*3	HOM	29.1	Takada et al., 2016
NM_016123.4:c.144C>G:NP_057207.2:p.Y48*	COMP HET	37	Ku et al., 2007
NM_016123.4:c.161G>A:NP_057207.2:p.R54K	HOM	34	Gokturk et al., 2018
NM_016123.4:c.228_230del:NP_057207.2:p.T77del	COMP HET	22.1	Andres et al., 2013
NM_016123.4:c.255_260dup:NP_057207.2:p.D86_L87dup	COMP HET	21	Grazioli et al., 2016
NM_016123.4:c.524del:NP_057207.2:p.N175Mfs*31	HOM	25.7	Enders et al., 2004
NM_016123.4:c.547C>T:NP_057207.2:p.R183*	COMP HET	35	Picard et al., 2010
NM_016123.4:c.574del:NP_057207.2:p.p.M192Wfs*14	HOM	23.3	Enders et al., 2004
NM_016123.4:c.593del:NP_057207.2:p.G198Efs*8	COMP HET	32	Bouma et al., 2009
NM_016123.4:c.623_624delCA:NP_057207.2:p.T208Nfs*12	COMP HET	23	Medvedev et al., 2003
NM_016123.4:c.631del:NP_057207.2:p.A211Qfs*2	COMP HET	24	Ku et al., 2007
NM_016123.4:c.821del:NP_057207.2:p.L274Pfs*14	HOM	32	Picard et al., 2003
NM_016123.4:c.823del:NP_057207.2:p.S275Lfs*13	COMP HET	29.9	Karananou et al., 2020
NM_016123.4:c.831+5G>T	COMP HET	22.3	Hoarau et al., 2007
NM_016123.4:c.877C>T:NP_057207.2:p.Q293*	HOM	40	Picard et al., 2010
NM_016123.4:c.893G>A:NP_057207.2:p.G298D	COMP HET	28.6	Bouma et al., 2009
NM_016123.4:c.897_900del:NP_057207.2:p.N300Ffs*44	COMP HET	33	Picard et al., 2010
NM_016123.4:c.1079T>A:NP_057207.2:p.L360*	HOM	39	Maglione et al., 2014
NM_016123.4:c.1126-1G>T	COMP HET	35	Maglione et al., 2014
NM_016123.4:c.1146del:NP_057207.2:p.G383Dfs*15	COMP HET	32	Grazioli et al., 2016
NM_016123.4:c.1188+520A>G	COMP HET	5.529	Ku et al., 2007
NM_016123.4:c.1189-1G>T	COMP HET	34	Ku et al., 2007
NM_016123.4:c.1204G>T:NP_057207.2:p.E402*	HOM	44	Picard et al., 2010; Cardenes et al., 2006
NM_016123.4:c.1240dup:NP_057207.2:p.I414Nfs*2	COMP HET	26.5	Ku et al., 2007
NM_016123.4:c.1290C>G:NP_057207.2:p.Y430*	COMP HET	37	Maglione et al., 2014
NM_016123.4:c.942-1481_1125+547del	COMP HET	NA	Ku et al., 2007
NM_016123.4:c.-9-1087_63del	HOM	NA	Ku et al., 2007

COMP HET: Compound Heterozygous, HOM: Homozygous.

(Andres et al., 2013; Bouma et al., 2009; Cardenes et al., 2006; Enders et al., 2004; Gokturk et al., 2018; Grazioli et al., 2016; Hoarau et al., 2007; Karananou et al., 2020; Ku et al., 2007; Maglione et al., 2014; Medvedev et al., 2003; Nishimura et al., 2021; Picard et al., 2003; Picard et al., 2010; Takada et al., 2016)

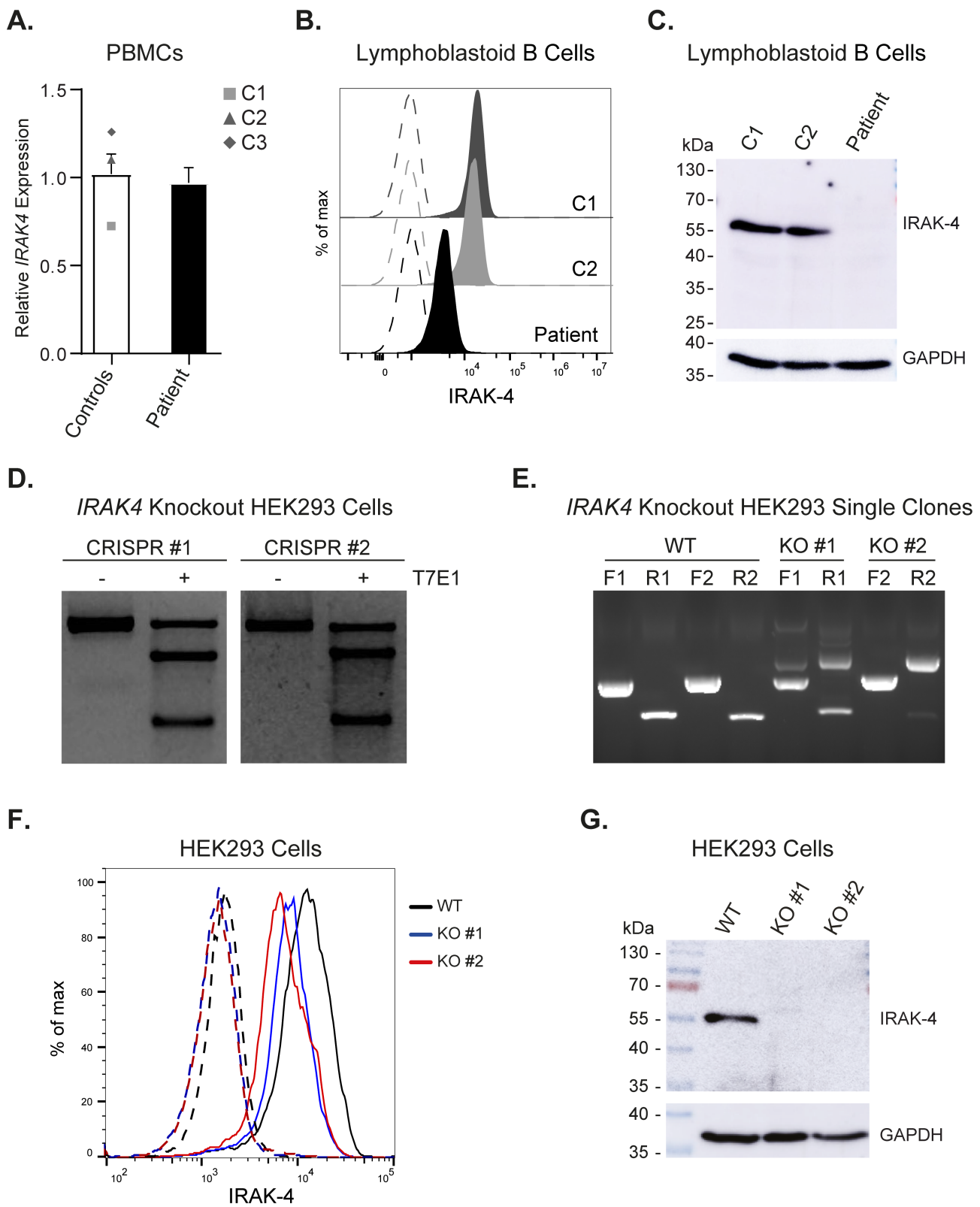


Fig. S1. A. Bar graph showing *IRAK4* levels normalized against *HPRT1* expression by RT-qPCR on PBMCs from the patient and three healthy controls (C1, C2, and C3). Relative *IRAK4* expression was calculated by normalization against the mean value for control cells, which is set to 1. The values shown are the mean \pm SEM of two independent experiments performed in duplicates. **B.** Histogram showing intracellular *IRAK4* expression in lymphoblastoid B cells generated from peripheral blood cells of the patient and two healthy controls (C1 and C2) as previously described (Belkaya et al., 2019). Dashed lines show unstained controls. **C.** Representative immunoblot image showing *IRAK4* and GAPDH expression in lymphoblastoid B cells from C1, C2, and Patient. **D.** Agarose gel electrophoresis of T7E1 assay results for CRISPR #1 and CRISPR #2. Lanes are grouped by CRISPR system and show bands for WT and knockout cells. **E.** Agarose gel electrophoresis of T7E1 assay results for WT and two knockout clones (KO #1 and KO #2). Lanes are grouped by clone and show bands for F1 and R1 cell lines. **F.** Histogram of intracellular *IRAK4* expression in HEK293 cells. WT cells show a peak around 10^3 . Knockout clones #1 and #2 show a shift towards higher expression, peaking around 10^4 . **G.** Western blot showing *IRAK4* and GAPDH expression in HEK293 cells. Lanes are labeled WT, KO #1, and KO #2. The WT lane shows a prominent band for *IRAK4* at ~ 55 kDa, which is absent in the knockout lanes.

4 expression in whole cell lysates (75 µg protein/lane) from lymphoblastoid B cells of the patient and two healthy controls (C1 and C2). Immunoblotting was performed with the IRAK-4 antibody, followed by GAPDH antibodies after stripping of the membrane, respectively. **D, E.** Agarose gel images showing T7 Endonuclease I assay (T7E1) on *IRAK4* knockout in HEK293 cells (**D**) and competitive PCR assay on *IRAK4* knockout single clones of HEK293 cells (KO #1 and KO #2, generated by CRISPR #1 and CRISPR #2 primer sets, respectively) (**E**). Primers used for CRISPR #1 (indicated by F1 and R1) and CRISPR #2 (indicated by F2 and R2) were listed in TableS1. **F.** Histogram showing intracellular IRAK-4 expression in WT and *IRAK4* knockout single clones of HEK293 cells (KO #1 and KO #2) by flow cytometry. Dashed lines show unstained controls. **G.** Representative immunoblot image showing IRAK-4 expression in whole cell lysates (75 µg protein/lane) from WT, KO #1 and KO #2 HEK293 cells. Immunoblotting was performed with the IRAK4 antibody, followed by GAPDH antibodies after stripping of the membrane, respectively. Expected molecular weights: IRAK-4; ~55 kDa, GAPDH: ~36 kDa.

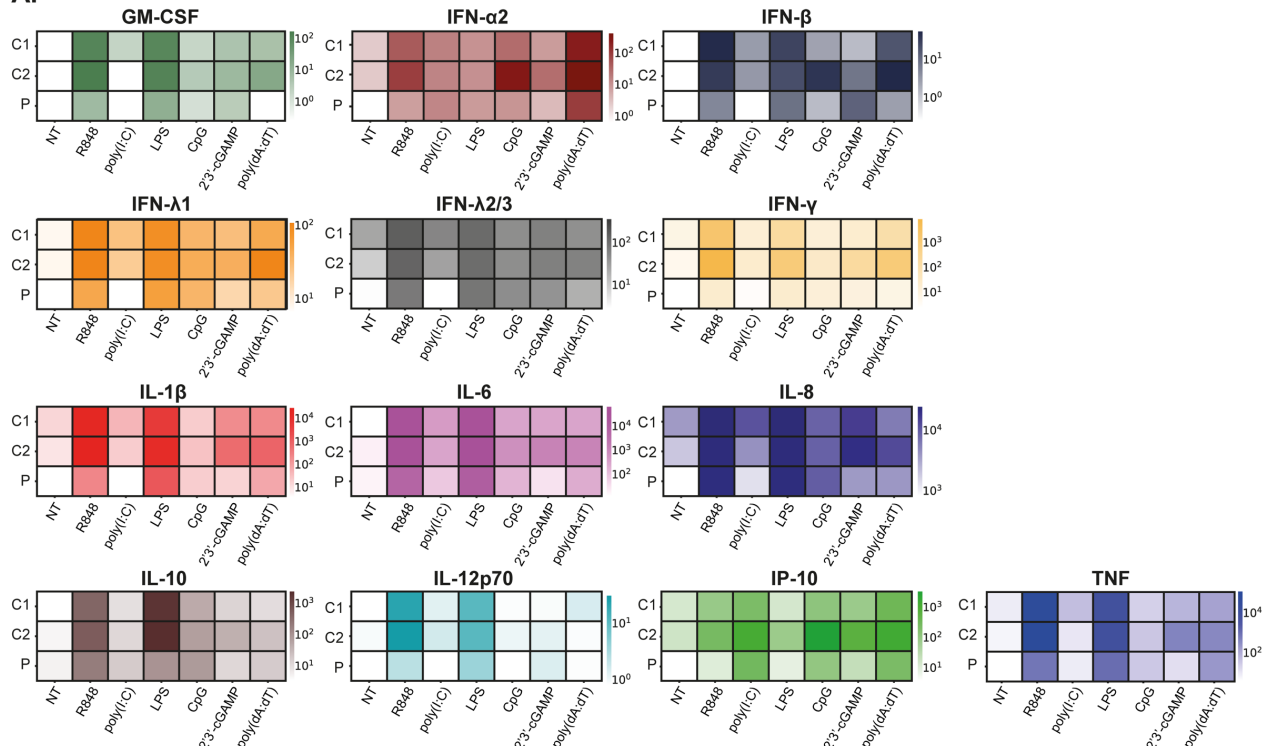
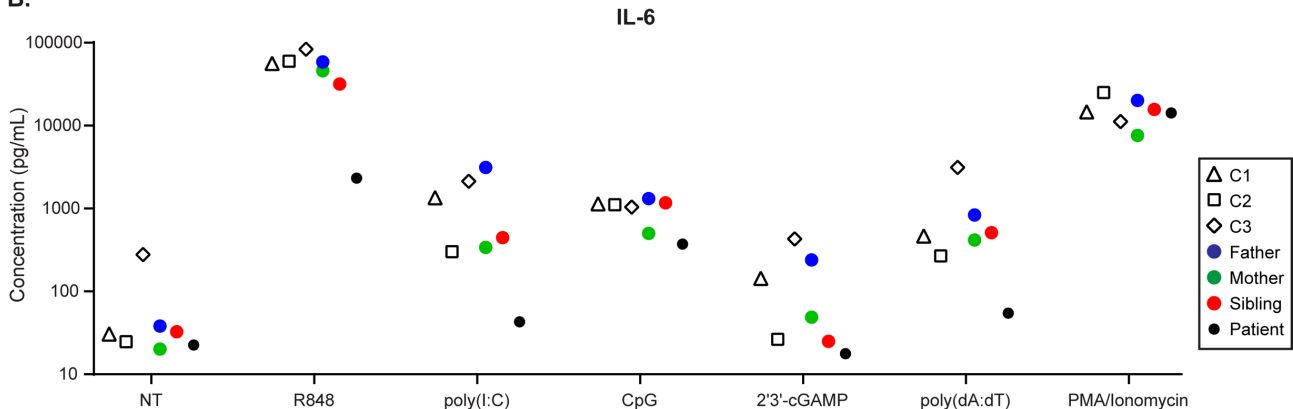
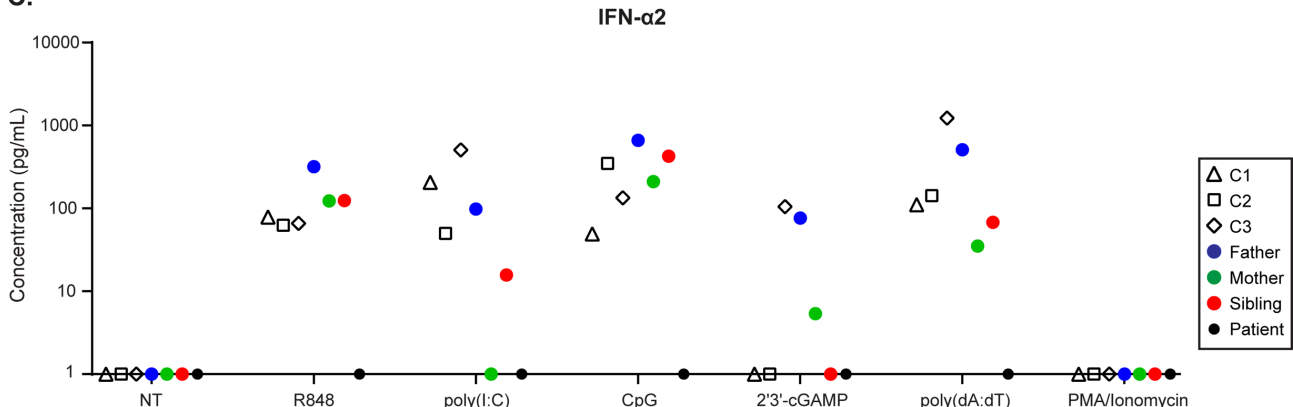
A.**B.****C.**

Fig. S2. A. Heatmap presentation of multiplex cytokine profiling showed as bar graphs in the Figure 6. Each heatmap represents a different cytokine. Color schemes showing the mean expression levels (pg/mL) from two independent experiments are presented on a logarithmic scale with base of 10. C1 and C2 are healthy controls, P is the patient. **B-C.** Graphs show IL-6 (**B**) and IFN- α 2 (**C**) production, measured by ELISA, from PBMCs of three healthy controls (C1, C2 and C3; open shapes), the patient

(black circle), and his father (blue circle), mother (green circle) and sibling (red circle) upon various stimuli. Values are of the mean levels of a single experiment performed in duplicates. NT: No treatment (Medium only).

References

- Andres, O., K. Strehl, U. Kolsch, S. Kunzmann, A.H. Lebrun, T. Stroh, K. Schwarz, H. Morbach, H. von Bernuth, and J. Liese. 2013. Even in pneumococcal sepsis CD62L shedding on granulocytes proves to be a reliable functional test for the diagnosis of interleukin-1 receptor-associated kinase-4 deficiency. *Pediatr Infect Dis J* 32:1017-1019.
- Belkaya, S., E. Michailidis, C.B. Korol, M. Kabbani, A. Cobat, P. Bastard, Y.S. Lee, N. Hernandez, S. Drutman, Y.P. de Jong, E. Vivier, J. Bruneau, V. Beziat, B. Boisson, L. Lorenzo-Diaz, S. Boucherit, M. Sebagh, E. Jacquemin, J.F. Emile, L. Abel, C.M. Rice, E. Jouanguy, and J.L. Casanova. 2019. Inherited IL-18BP deficiency in human fulminant viral hepatitis. *J Exp Med* 216:1777-1790.
- Berendsen, H.J.C., J.P.M. Postma, W.F. van Gunsteren, A. DiNola, and J.R. Haak. 1984. Molecular dynamics with coupling to an external bath. *J. Chem. Phys.* 81:
- Bouma, G., R. Doffinger, S.Y. Patel, E. Peskett, J.C. Sinclair, G. Barcenas-Morales, L. Cerron-Gutierrez, D.S. Kumararatne, E.G. Davies, A.J. Thrasher, and S.O. Burns. 2009. Impaired neutrophil migration and phagocytosis in IRAK-4 deficiency. *Br J Haematol* 147:153-156.
- Cardenes, M., H. von Bernuth, A. Garcia-Saavedra, E. Santiago, A. Puel, C.L. Ku, J.F. Emile, C. Picard, J.L. Casanova, E. Colino, A. Bordes, A. Garfia, and C. Rodriguez-Gallego. 2006. Autosomal recessive interleukin-1 receptor-associated kinase 4 deficiency in fourth-degree relatives. *J Pediatr* 148:549-551.
- Enders, A., U. Pannicke, R. Berner, P. Henneke, K. Radlinger, K. Schwarz, and S. Ehl. 2004. Two siblings with lethal pneumococcal meningitis in a family with a mutation in Interleukin-1 receptor-associated kinase 4. *J Pediatr* 145:698-700.
- Essmann, U., L. Perera, and M.L. Berkowitz. 1995. A smooth particle mesh Ewald method. *J. Chem. Phys.* 103:
- Gokturk, B., J.L. Casanova, C. Picard, D. Cagdas Ayvaz, B. Erman, I. Tezcan, H. Ozdemir, A. Ozel, and I. Reisli. 2018. A Novel Homozygous Mutation With Different Clinical Presentations in 2 IRAK-4-Deficient Siblings: First Case With Recurrent Salmonellosis and Non-Hodgkin Lymphoma. *J Investig Allergol Clin Immunol* 28:271-273.
- Grazioli, S., S.J. Hamilton, M.L. McKinnon, K.L. Del Bel, L. Hoang, V.E. Cook, K.J. Hildebrand, A.K. Junker, and S.E. Turvey. 2016. IRAK-4 deficiency as a cause for familial fatal invasive infection by Streptococcus pneumoniae. *Clin Immunol* 163:14-16.
- Hoarau, C., B. Gerard, E. Lescanne, D. Henry, S. Francois, J.J. Lacapere, J. El Benna, P.M. Dang, B. Grandchamp, Y. Lebranchu, M.A. Gougerot-Pocidalo, and C. Elbim. 2007. TLR9 activation induces normal neutrophil responses in a child with IRAK-4 deficiency: involvement of the direct PI3K pathway. *J Immunol* 179:4754-4765.
- Huang, J., S. Rauscher, G. Nawrocki, T. Ran, M. Feig, B.L. de Groot, H. Grubmuller, and A.D. MacKerell, Jr. 2017. CHARMM36m: an improved force field for folded and intrinsically disordered proteins. *Nat Methods* 14:71-73.
- Humphrey, W., A. Dalke, and K. Schulten. 1996. VMD: visual molecular dynamics. *J Mol Graph* 14:33-38, 27-38.
- Jordi, M., J. Marty, V. Mordasini, A. Lunemann, S. McComb, M. Bernasconi, and D. Nadal. 2017. IRAK4 is essential for TLR9-induced suppression of Epstein-Barr virus BZLF1 transcription in Akata Burkitt's lymphoma cells. *PLoS One* 12:e0186614.
- Jorgensen, W.L., J. Chandrasekhar, and J.D. Madura. 1983. Comparison of simple potential functions for simulating liquid water. *J. Chem. Phys.* 79:
- Karananou, P., A. Alataki, and E. Papadopoulou-Alataki. 2020. Interleukin-1 Receptor-Associated Kinase 4 Deficiency in a Greek Teenager. *Case Reports Immunol* 2020:8846827.
- Ku, C.L., H. von Bernuth, C. Picard, S.Y. Zhang, H.H. Chang, K. Yang, M. Chrabieh, A.C. Issekutz, C.K. Cunningham, J. Gallin, S.M. Holland, C. Roifman, S. Ehl, J. Smart, M. Tang, F.J. Barrat, O. Levy, D. McDonald, N.K. Day-Good, R. Miller, H. Takada, T. Hara, S. Al-Hajjar, A. Al-Ghonaium, D. Speert, D. Sanlaville, X. Li, F. Geissmann, E. Vivier, L. Marodi, B.Z. Garty, H. Chapel, C. Rodriguez-Gallego, X. Bossuyt, L. Abel, A. Puel, and J.L. Casanova. 2007.

- Selective predisposition to bacterial infections in IRAK-4-deficient children: IRAK-4-dependent TLRs are otherwise redundant in protective immunity. *J Exp Med* 204:2407-2422.
- Lin, S.C., Y.C. Lo, and H. Wu. 2010. Helical assembly in the MyD88-IRAK4-IRAK2 complex in TLR/IL-1R signalling. *Nature* 465:885-890.
- Maglione, P.J., N. Simchoni, S. Black, L. Radigan, J.R. Overbey, E. Bagiella, J.B. Bussel, X. Bossuyt, J.L. Casanova, I. Meyts, A. Cerutti, C. Picard, and C. Cunningham-Rundles. 2014. IRAK-4 and MyD88 deficiencies impair IgM responses against T-independent bacterial antigens. *Blood* 124:3561-3571.
- McGibbon, R.T., K.A. Beauchamp, M.P. Harrigan, C. Klein, J.M. Swails, C.X. Hernandez, C.R. Schwantes, L.P. Wang, T.J. Lane, and V.S. Pande. 2015. MDTraj: A Modern Open Library for the Analysis of Molecular Dynamics Trajectories. *Biophys J* 109:1528-1532.
- Medvedev, A.E., A. Lentschat, D.B. Kuhns, J.C. Blanco, C. Salkowski, S. Zhang, M. Arditi, J.I. Gallin, and S.N. Vogel. 2003. Distinct mutations in IRAK-4 confer hyporesponsiveness to lipopolysaccharide and interleukin-1 in a patient with recurrent bacterial infections. *J Exp Med* 198:521-531.
- Nishimura, S., Y. Kobayashi, H. Ohnishi, K. Moriya, M. Tsumura, S. Sakata, Y. Mizoguchi, H. Takada, Z. Kato, V. Sancho-Shimizu, C. Picard, S.R. Irani, O. Ohara, J.L. Casanova, A. Puel, N. Ishikawa, S. Okada, and M. Kobayashi. 2021. IRAK4 Deficiency Presenting with Anti-NMDAR Encephalitis and HHV6 Reactivation. *J Clin Immunol* 41:125-135.
- Picard, C., A. Puel, M. Bonnet, C.L. Ku, J. Bustamante, K. Yang, C. Soudais, S. Dupuis, J. Feinberg, C. Fieschi, C. Elbim, R. Hitchcock, D. Lammas, G. Davies, A. Al-Ghonaium, H. Al-Rayes, S. Al-Jumaah, S. Al-Hajjar, I.Z. Al-Mohsen, H.H. Frayha, R. Rucker, T.R. Hawn, A. Aderem, H. Tufenkeji, S. Haraguchi, N.K. Day, R.A. Good, M.A. Gougerot-Pocidalo, A. Ozinsky, and J.L. Casanova. 2003. Pyogenic bacterial infections in humans with IRAK-4 deficiency. *Science* 299:2076-2079.
- Picard, C., H. von Bernuth, P. Ghadil, M. Chrabieh, O. Levy, P.D. Arkwright, D. McDonald, R.S. Geha, H. Takada, J.C. Krause, C.B. Creech, C.L. Ku, S. Ehl, L. Marodi, S. Al-Muhsen, S. Al-Hajjar, A. Al-Ghonaium, N.K. Day-Good, S.M. Holland, J.I. Gallin, H. Chapel, D.P. Speert, C. Rodriguez-Gallego, E. Colino, B.Z. Garty, C. Roifman, T. Hara, H. Yoshikawa, S. Nonoyama, J. Domachowske, A.C. Issekutz, M. Tang, J. Smart, S.E. Zitnik, C. Hoarau, D.S. Kumararatne, A.J. Thrasher, E.G. Davies, C. Bethune, N. Sirvent, D. de Ricaud, Y. Camcioglu, J. Vasconcelos, M. Guedes, A.B. Vitor, C. Rodrigo, F. Almazan, M. Mendez, J.I. Arostegui, L. Alsina, C. Fortuny, J. Reichenbach, J.W. Verbsky, X. Bossuyt, R. Doffinger, L. Abel, A. Puel, and J.L. Casanova. 2010. Clinical features and outcome of patients with IRAK-4 and MyD88 deficiency. *Medicine (Baltimore)* 89:403-425.
- Schymkowitz, J., J. Borg, F. Stricher, R. Nys, F. Rousseau, and L. Serrano. 2005. The FoldX web server: an online force field. *Nucleic Acids Res* 33:W382-388.
- Takada, H., M. Ishimura, T. Takimoto, T. Kohagura, H. Yoshikawa, M. Imaizumi, K. Shichijyou, Y. Shimabukuro, T. Kise, N. Hyakuna, O. Ohara, S. Nonoyama, and T. Hara. 2016. Invasive Bacterial Infection in Patients with Interleukin-1 Receptor-associated Kinase 4 Deficiency: Case Report. *Medicine (Baltimore)* 95:e2437.
- van Zundert, G.C.P., J. Rodrigues, M. Trellet, C. Schmitz, P.L. Kastritis, E. Karaca, A.S.J. Melquiond, M. van Dijk, S.J. de Vries, and A. Bonvin. 2016. The HADDOCK2.2 Web Server: User-Friendly Integrative Modeling of Biomolecular Complexes. *J Mol Biol* 428:720-725.
- Xue, L.C., J.P. Rodrigues, P.L. Kastritis, A.M. Bonvin, and A. Vangone. 2016. PRODIGY: a web server for predicting the binding affinity of protein-protein complexes. *Bioinformatics* 32:3676-3678.